

## **General Disclaimer**

### **One or more of the Following Statements may affect this Document**

- This document has been reproduced from the best copy furnished by the organizational source. It is being released in the interest of making available as much information as possible.
- This document may contain data, which exceeds the sheet parameters. It was furnished in this condition by the organizational source and is the best copy available.
- This document may contain tone-on-tone or color graphs, charts and/or pictures which have been reproduced in black and white.
- This document is paginated as submitted by the original source.
- Portions of this document are not fully legible due to the historical nature of some of the material. However, it is the best reproduction available from the original submission.

SPT

NASA Technical Memorandum 82933

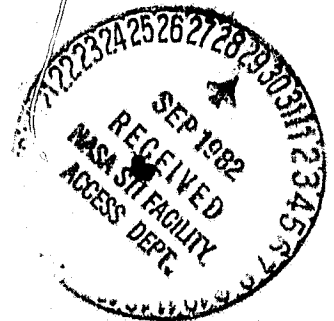
# A Study of the Nature of Solid Particle Impact and Shape on the Erosion Morphology of Ductile Metals

(NASA-TM-82933) A STUDY OF THE NATURE OF SOLID PARTICLE IMPACT AND SHAPE ON THE EROSION MORPHOLOGY OF DUCTILE METALS (NASA)  
19 p HC A02/MF A01 CSCI 11F

N82-33493

G3/26 Unclas 35045

✓ P. Veerabhadra Rao, Stanley G. Young, and Donald H. Buckley  
*Lewis Research Center  
Cleveland, Ohio*



Prepared for the  
Microscopy of the Degradation of Materials (Wear and Erosion),  
MICRO 82, International Symposium and Exhibition  
sponsored by the Royal Microscopical Society  
London, England, July 12-16, 1982



A STUDY OF THE NATURE OF SOLID PARTICLE IMPACT AND SHAPE ON THE EROSION  
MORPHOLOGY OF DUCTILE METALS

by P. Veerabhadra Rao, Stanley G. Young, and Donald H. Buckley

Lewis Research Center  
National Aeronautics and Space Administration  
Cleveland, Ohio 44135

SUMMARY

E-1298  
Studies were conducted to identify the differences in the modes of erosion between impulsive and steady-jet glass bead erodant particle impingement at normal incidence. A 6061-T6 aluminum alloy, copper and 1045 steel were used as test materials. A small muzzle gas gun apparatus was used for impulse testing and a commercial sand blasting facility was used for steady-jet impingement testing. Crushed glass was also used as an erodant in the steady-jet apparatus and the erosion patterns from crushed glass were compared with those of glass bead impingement erosion.

Morphological features and material removal mechanisms for the specimens were studied using weight loss measurements, scanning electron microscope, energy dispersive X-ray spectroscopy (EDS), and surface profilometry. Impulsive conditions induced more severe damage and resulted in embedment and fragmentation of glass beads, likely due to more intense pressure pulses and longer loading times on impact. Patterns from steady-jet glass bead impingement experiments exhibited overlapping of plastically deformed craters with very little evidence of particle fragmentation.

Recorded profiles and micrographs of the steady-jet impingement specimens indicate that crushed glass induced deeper and wider pits than glass beads. The volume loss of 1045 steel was almost half that observed on aluminum and copper specimens with both types of erodant particles. The material removal process for glass bead impingement appears to be in the form of deformation induced fatigue failure with flake-like debris visible at high magnification. With crushed glass material appears to have been removed as small chips, leaving a jagged, angular, faceted surface characteristic of "cutting wear".

EDS analyses indicated traces of silicon (from the erodant particles) on all three materials. Silicon amounts were maximum at the pit bottom (center).

1. INTRODUCTION

Erosion of metallic and nonmetallic materials by solid particle impingement has been investigated for many years. Recently emphasis has been given to problems involving erosion of aircraft compressor and turbine blades due to sand and dust, exhaust ducts and rocket nozzles due to the combustion products in both solid and liquid propellents, coal gasification machinery by ash particles and in numerous other applications (Adler, 1979; Schmitt, 1980).

Studies of multiple particle impact erosion of ductile materials have been made using weight loss measurements as well as light optical, and electron microscopy (Ives & Ruff, 1977; Ruff, 1980; Bellman & Levy, 1981; Rickerby & Macmillan, 1980). In single and multiple particle impact investiga-

## ORIGINAL FACTS OF POOR QUALITY

tions, parameters such as the velocity of impact, angle of impact, particle size and particle shape have been studied (e.g., Head and Harr, 1970; Hutchings, 1977; Tilly, 1979). As a result of these studies, several equations (e.g., Finnie, 1960; Bitter, 1963a,b; Rabinowicz, 1979), models (Head, et al., 1973; Jennings, et al., 1975; Hutchings, 1981) and suggested mechanisms (Hutchings, 1977; Christman & Shewmon, 1979; Finnie, et al., 1979; Carter, et al., 1980; Brainard & Salik, 1980; Brown, et al., 1981) for the material removal process have been developed. In most studies, material removal is related to the formation of small platelets (e.g. Ruff, 1980; Bellman & Levy, 1981; Brown, et al., 1981; Hutchings, 1981). This observation is particularly noticeable when spherical erodant particles are used. This has generally been referred to as "deformation wear" resulting from repeated impact plastic flow, extrusion, low cycle fatigue and final failure. Conversely, angular particles leave sharp-edged, jagged patterns on the material surfaces (Hutchings, 1977; Salik & Buckley, 1981a). This has generally been referred to as "cutting wear" in solid impingement erosion studies. Erosion attack in most engineering situations is not steady, but rather is believed to be random and irregular. Hence, comparisons of different erosion attack modes - steady and impulsive - under laboratory conditions should help in the better understanding the erosion process.

Many attempts have been made to correlate the erosion resistance of various materials with material properties. Some studies suggest that erosion resistance increases with hardness for ductile materials (Finnie, et al., 1967; Sheldon, 1977; Tilly, 1969a,b; Wood & Espenschade, 1965). Some studies, however, did not show direct relationships with hardness after various heat treatments (Salik & Buckley, 1981b; Salik, et al., 1981) including one by Finnie, et al. (1967). In fact, work hardening of pure metals, viz., aluminum, silver, copper and nickel, resulted in a substantial increase in hardness without significant change in erosion resistance; whereas for two steels a slight decrease in the erosion resistance was observed although hardness increased after heat treatment (Finnie, et al.). Levy (1979) postulated that as the localized ductility of a material increases, the erosion resistance increases even though its hardness and strength decrease. On the other hand, Hutchings (1981) states that high values of dynamic hardness and ductility are needed for good resistance to erosion of ductile materials. Levy cautions that there appears to be a finite region of behavior for each base metal where its erosion varies as its ductility. Other properties used for correlations have been: "thermal pressure" defined as the product of the linear thermal expansion coefficient, the temperature rise required for melting, the bulk modulus of the metal (Ascarelli, 1971); melting point (Smeltzer, et al. 1970); ductility at fracture (Tilly, 1969a, 1979); product of hardness and elongation (Wood & Espenschade, 1965); elastic modulus (Brauer & Kriegel, 1965; Tuitt, 1974); the product of density, specific heat and temperature rise required for melting (Hutchings, 1975); the cube root of the mean molecular weight divided by the thermal conductivity, the melting temperature, the enthalpy of melting, and the cube root of the density of the metal (Jennings et al., 1975); interatomic bond energy (Vijh, 1976); and ultimate resilience (defined as tensile strength squared divided by two times the elastic modulus (Eyre, 1976). Jones and Lewis (1979) compared the erosion wear rate of several alloy steels with impact strength, ultimate tensile strength, fracture toughness, elongation, hardness and coefficient of linear expansion. They found that using physical parameters was clearly inadequate in efforts to represent erosion resistance of alloy steels. They

observed a direct relationship between erosion and linear thermal expansion, whereas Ascarelli (1971) observed erosion as inversely proportional to linear thermal expansion for pure metals. Malkin (1981) proposed a new correlation of the specific erosion energy (the kinetic energy per unit volume of metal removed) with the specific melting energy (melting energy per unit volume of target metal) using an analogy with grinding. Most recently Soderberg, et al. (1982) stated that surface layer hardness and ductility are the most important material properties for cutting erosion resistance and deformation erosion resistance, respectively. In spite of all these attempts, there is still no universally agreed-upon property which correlates well with the erosion resistances of a wide spectrum of ductile metallic materials.

The objectives of this study were to investigate the differences in erosion mechanisms of ductile materials caused by two different impingement modes and two different types of erodant particles. In this investigation spherical glass beads were impinged on metal targets with a single impulse gas gun and with a steady-jet stream; crushed glass particles were also impinged on metal targets with a steady-jet stream. All studies were conducted at normal impact. The similarities and differences in the erosion patterns were observed with scanning electron microscopy (SEM), surface profilometry, and energy dispersive X-ray spectroscopy (EDS).

## 2. MATERIALS, APPARATUS AND PROCEDURE

### 2.1 Materials

Specimens of the aluminum alloy 6061-T6, copper and 1045 steel were used in this investigation. These three materials were studied in previous impingement tests (Brainard & Salik, 1980; Salik, et al., 1981) and were selected for this study for comparative purposes. The aluminum and copper specimens were 6 mm thick, 25 mm wide and 37.5 mm long. These were tested as received. The specimens of 1045 steel were 25 mm diameter cylinders approximately 13 mm long.

The steel specimens were annealed by heating to 740° C, furnace cooling to 650° C and cooling to room temperature in still air prior to testing (Salik & Buckley, 1981). Impingement of particles was on the flat face of the specimens. The nominal compositions and mechanical properties of all the materials are presented in Tables I and II. Before erosion exposure, all specimens were polished with 600-grit emery paper, then with 3 micrometer diamond paste, cleaned with distilled water, and air dried.

### 2.2 Apparatus and Procedure

The investigations in this report were conducted with an impulse impingement gas-gun apparatus and a commercial sand-blasting facility. A schematic of the gun apparatus is shown in figure 1 and a schematic of the nozzle arrangement of sand-blasting facility is shown in figure 2.

In the impulse impingement facility a teflon sabot, which contains 4 cubic mm of spherical glass beads, is accelerated in the muzzle by a surge of argon to a pressure of approximately 21 MPa. The sabot is trapped in the muzzle and the glass beads are ejected at an average velocity estimated at 140 m/sec. The targets were mounted in a holder with the surface normal to impact. The velocity of the glass bead charge was measured by a photo-optical gate assembly using a steel ball for calibration.

The sand-blasting facility was used to continuously impact the specimens at normal incidence. Commercial grade No. 5 spherical glass beads of approximately 20 micrometers average diameter were used in both facilities. In the sand-blasting facility the distance between the specimen and the nozzle (diameter 1.18 mm) was 13 millimeters. Argon was used as the driving gas at a pressure of approximately 0.54 MPa. At this pressure, the velocity of the jet is assumed to be 60 to 80 m/sec (Ruff & Ives, 1975). The jet divergence was about 2 degrees relative to the center line and the bead flow was approximately 0.76 grams per second.

Volume loss values were obtained by weighing specimens before and after exposure to the erodants and dividing by density. Surface profiles of the eroded surfaces were recorded with a profilometer. The eroded surfaces were observed with a scanning electron microscope (SEM) and chemical analyses were obtained by means of energy dispersive X-ray spectroscopy (EDS).

### 3. RESULTS AND DISCUSSION

#### 3.1 Impulsive vs Steady-jet Impingement Modes

Figures 3 and 4 present SEM micrographs of aluminum specimens exposed to impulsive impact and steady-jet impingement. With impulsive impact, individual circular craters are observed which contain small slabs, mostly pieces of glass beads which shattered on impact (Brainard & Salik, 1980). The small pieces that were blasted away from the surface may have caused "cutting wear" due to subsequent outflow (Tilly, 1973).

Under steady-jet impingement with glass bead erodant particles, overlapping deformation pits are observed which contain little or no slab-like debris (see fig. 3(b)) as seen in impulsive impact. Material appears to have been removed in the form of very small flakes or platelets (fig. 4). The differences in damage patterns between the two forms of attack may be attributed to two factors. First, the higher velocity of impulse impingement results in a more intense impact causing more plastic deformation and flow than steady-jet impingement; and secondly, the solid-solid impact is believed to have a longer contact time (on the order of hundreds of microseconds) than for other types of impingement tests including cavitation (Bowden & Field, 1964). Embedment and fragmentation of glass beads during impulsive conditions further increase the contact time.

The two-stage erosion process due to direct impact and cutting by radial outflow by angular particles proposed by Tilly, (1973) may not apply for the case of spherical glass beads. This is due to the fact that most glass beads were not fragmented in this study, and therefore lack the cutting aspect of erosion. Considerations of initial impact should be supplemented by considerations of dragging, spinning, extrusion and fatigue effects during the radial outflow of the glass beads.

#### 3.2 Erosion Wear by Spherical Glass Beads

Figures 5 to 7 present micrographs of the aluminum, copper and 1045 steel specimens eroded by spherical glass beads for 10 minute steady-jet exposures at 0.54 MPa argon gas pressure. Volume losses for these materials are listed in Table III. Figures 5(a), 6(a), and 7(a) show the pit shapes and resulting erosion patterns on the surface. The erosion patterns have been divided into five regions (Rao, et.al., 1982a). Region 1, the central zone, is composed of radial deformation tracks, emanating from the center of

the impact crater. Region 2 contains both radial tracks and concentric rings. Region 3, contains only radial tracks. Region 4 is a rough surface with irregular concentric ripples, and region 5 is the outer transition zone from region 4 to the undamaged metal. The five different regions are observed on aluminum and copper, but the steel specimen (fig. 7(a)) does not show the concentric rings as seen in region 2 of the other materials. The erosion pattern is believed to still be developing. Pit bottoms, concentric rings, and pit edges are shown in figures 5, 6, and 7 ((b), (c) and (d), respectively).

There are many similarities between the erosion patterns for all three materials. The flake-like debris as shown in figure 4 was observed in all three materials. These thin flakes as mentioned earlier are believed to be formed by cyclic stresses, deformation, extrusion, and fatigue failure resulting in volume loss. Because the surface is not jagged and angular it appears that deformation (as opposed to cutting) wear predominates in the process of erosion wear with glass beads. This observation agrees well with experiments of Bitter (1963a,b), who used angular particles. In this reference total wear was determined to be the summation of deformation wear and cutting wear; but the "cutting wear" appeared to be absent at normal incidence for soft, ductile materials.

### 3.3 Erosion Wear by Crushed Glass

Figures 8 to 10 present micrographs of the overall view, the pit bottom, slopes, and edges for the three materials exposed to crushed glass particle impingement for 10 minutes. Figures 8(a) and 9(a) show a pattern which has been divided into four regions by Rao, et.al., (1982b): region 1, pit bottom with no clear pattern; region 2, concentric ripple patterns on the sides of the pit; region 3, a rough undulating region with a changing slope from almost vertical to horizontal; and region 4, the transition from slight damage to the undamaged area of the specimen.

The steel specimen (fig. 10(a)), however, did not show any ripples on the side of the pit. From table III it can be seen that the volume loss of steel is less than half that for either aluminum or copper. All surfaces of the test specimens exhibit jagged, angular patterns (figs. 8 to 10) which is an indication of the predominance of "cutting wear" (as opposed to deformation wear).

### 3.4 Comparison of Erosion Wear Between Glass Beads and Crushed Glass

Surface profile traces of all three materials after 10 minutes of glass bead impingement are presented in figure 11 and with 10 minutes of crushed glass impingement in figure 12. The profiles in figure 12, resulting from crushed glass impingement are wider, deeper and result in an overall smoother surfaces than the same in figure 11. The small steps (concentric rings), visible on the pit slopes in region 2 for aluminum and copper are more pronounced than the same in figure 12. because of the scale distortion of the surface profiles and deep pits of figures 11 and 12, metallographic cross sections of the specimens are shown in figure 13 to show the overview of the pit. The pit bottoms are wider for crushed glass impingement than for glass beads. These effects are probably due to the increased cutting capability of the crushed glass.

All material surfaces were analyzed using energy dispersive X-ray spectroscopy (EDS) after erosion exposure. Analyses were made at the pit

bottom, edge of the pit and at the metal surface far away from the pit. The results are shown in figures 14 and 15.

The silicon and calcium peaks in figure 14(a) (at the pit bottoms) show that elements which were present in the glass beads have transferred to the surfaces of all impacted materials. The silicon/metal peak ratio drops as the distance from the center of impact increases. Observations of impacted glass beads at higher magnifications, and of glass beads collected after testing, indicated that most beads were not broken but were still spherical (Rao, et al., 1982a). As a result of these apparently conflicting observations, it could be presumed that either a glass bead loses some of its mass over much of its surface during impact, subsequent radial outflow and spinning, and/or other interacting mechanisms are involved. This possibility may be valid in light of the particle size distribution analyses carried out by Tilly (1973) who reported that particle sizes were, in general, considerably reduced after impingement compared to the size before impact. He has, however, attributed this observation to fragmentation. The extent of the fragmentation is dependent on initial particle size and velocity; bigger particles and higher velocities exhibit the most fragmentation. As mentioned earlier most glass beads were not fragmented in the present investigation due possibly to low impact velocity.

The analysis presented in figure 15 also indicates the presence of elements that were present in the crushed glass. Again, the pit bottoms (fig. 15(a)) contained the highest Si levels with decreasing amounts as distance increased from the center of the pit (in region 3). It is possible that fine, broken crushed glass particles are embedded or trapped in the rough surface. However, within the pit no individual glass particles could be identified. Several particles were observed outside the central pit. The concept of an embedded erodant particle layer on the material surface suggested by some investigators (Ives & Ruff, 1979; Kossel, et al., 1978, 1979) seems probable. However EDS analysis indicates that the chemistry is slightly different from that of the original impacting glass.

Another unexpected result was that the silicon peaks were higher for glass bead impingement than for crushed glass. The reasons for the above observations are not known, but it is suggested that these effects may be due to more complex chemical/mechanical interactions between the impacting particles and the target material than previously considered.

#### 4. CHARACTERIZATION AND DETERMINATION OF EROSION RESISTANCE

Erosion resistance can be defined as the ratio of the volume of impacting particles to the volume of material removed; the higher the ratio, the higher the erosion resistance. The volume losses of materials presented in table III were obtained with the same volume of either glass beads or crushed glass particles per unit time. The highest volume losses for copper and aluminum indicate least resistance to glass bead and crushed glass impingement erosion. Steel is the most resistant as expected because, in general, harder materials have been found to have higher erosion resistance with a few exceptions.

It is generally accepted that the energy absorbed by the material until it fails in tensile testing (defined as the area under the stress-strain curve) is a property which correlates roughly with cavitation erosion resistance of soft ductile materials, and it seems reasonable that this property could correlate with solid particle erosion resistance of ductile materials as well. However, a wide spectrum of ductile metallic materials

ORIGINAL PAGE IS  
OF POOR QUALITY

needs to be tested before arriving at a good material property, or a combination of properties for correlation purposes.

5. SUMMARY

A series of normal impact erosion experiments were conducted to compare the effects of two types of impingement modes and two types of erodant particles. Single impulse and continuous (steady-jet) impact studies were made with spherical glass beads, and steady-jet impact studies were also made with angular, crushed glass particles. Specimens of 6061-T6 aluminum, copper and 1045 steel were tested. The main findings of these studies are as follows:

1. Damage patterns from impulse experiments show larger, rounded individual craters containing fragments of glass beads which shattered on impact.

2. Damage patterns from steady-jet impingement show multiple smaller overlapping dents or craters with virtually no visible fragments. Glass beads were not broken in these tests.

3. Damage patterns from steady-jet impingement tests with crushed glass show jagged, angular surfaces which are indicative of "cutting wear" as opposed to deformation wear in the case of glass bead impact studies.

4. Erosion morphology of steady-jet glass bead impingement divides the erosion pit into five regions. Region 1, the central zone, is composed of radial deformation tracks, emanating from the center of the impact crater. Region 2 contains both radial tracks and concentric rings. Region 3 contains only radial tracks. Region 4 is a rough surface with irregular concentric ripples, and region 5 is the outer transition zone from region 4 to the undamaged area.

5. Erosion morphology of steady-jet crushed glass impingement divides the erosion pit into four regions. Region 1, pit bottom with no clear pattern. Region 2, concentric ripple patterns on the sides of the pit. Region 3, a rough undulating region with a changing slope from almost vertical to horizontal, and region 4, the transition from slight damage to the undamaged area.

6. The steel specimen suffered less than half the erosion experienced by both aluminum and copper. SEM and EDS analyses of the surfaces showed that for steady-jet impingement studies with both glass beads and crushed glass, silicon deposition was highest in pit centers.

REFERENCES

- Adler, W. F. (1979) Assessment of the state of knowledge pertaining to solid particle erosion. Rept. ETI-CR79-680, contract no. DAAG 29-77-C-0039, Effects Technology, Inc., Santa Barbara, Ca.
- Ascarelli, P. (1971) Relation between the erosion by solid particles and the physical properties of metals. AMMAC-TR-71-47, Army Materials and Mechanics Research Center, Watertown, Mass.
- Bellman, R. & Levy, A. V. (1981) Platelet mechanism of erosion of ductile metals. In: Wear of Materials, (Ed. by S. K. Rhee, A. W. Ruff & K. C. Ludema), p. 564. Ann. Soc. Mech. Engrs., New York.
- Bitter, J. G. A. (1963 a, b) A study of erosion phenomena - part I and II. Wear, 6, 5 & 169.

- Bowden, F. P. & Field, J. E. (1964) The brittle fracture of solids by liquid impact by solid impact, and by shock. Proc. Roy. Soc. London A. 282, 331.
- Brainard, W. A. & Salik, J. (1980) Scanning electron - microscope study of normal-impingement erosion of ductile metals. NASA TP-1609, National Aeronautics and Space Administration, Washington, D.C.
- Brauer, H. & Kriegel, E. (1965) Verschleiss von Rohrkrummern beim pneumatischen und hydraulischen Feststoff transport. (Erosion of pipe bends in pneumatic and hydraulic solids - transport.) Chem. Ingr. Tech. 37, 265.
- Brown, R., Jun, E. J. & Edington, J. W. (1981) Erosion of  $\alpha$ -Fe by spherical glass particles. Wear, 70, 347.
- Carter, G., Nobes, M. J. & Arshak, K. I. (1980) The mechanism of ripple generation on sandblasted ductile solids. Wear, 65, 151.
- Christman, T. & Shewmon, P. G. (1979) Adiabatic shear localization and erosion of strong aluminum alloys. Wear, 54, 145.
- Eyre, T. S. (1976) Wear characteristics of metals. Tribology Int. 9, 203.
- Finnie, I. (1960) Erosion of surfaces by solid particles. Wear, 3, 87.
- Finnie, I., Levy, A. & McFadden, D. H. (1977) Fundamental mechanisms of the erosive wear of ductile metals by solid particles. In: Erosion: Prevention and Useful Applications (Ed. by W. F. Adler), ASTM STP 664, p. 36. Am. Soc. Testing & Mats., Philadelphia, Pa.
- Finnie, I., Wolak, J. & Kabil, Y. (1967) Erosion of metals by solid particles. J. Materials, 2, 682.
- Head, W. J. & Harr, M. E. (1970) The development of a model to predict the erosion of materials by natural contaminants. Wear, 15, 1.
- Head, W. J., Lineback, L. D. & Mannings, C. R. (1973) Modification and extension of a model for predicting the erosion of ductile materials. Wear, 23, 291.
- Hutchings, I. M. (1975) Prediction of the resistance of metals to erosion by solid particles. Wear, 35, 371.
- Hutchings, I. M. (1977) Mechanisms of the erosion of metals by solid particles. In: Erosion: Prevention and Useful Applications (Ed. by W. F. Adler), ASTM STP 664, p. 59. Am. Soc. Testing & Mats., Philadelphia, Pa.
- Hutchings, I. M. (1981) A model for the erosion of metals by spherical particles at normal incidence. Wear, 70, 269.
- Ives, L. K. & Ruff, A. W. (1977) Electron microscope study of erosion damage in copper. In: Erosion: Prevention and Useful Applications (Ed. by W. F. Adler), ASTM STP 664, p. 5. Am. Soc. Testing & Mats., Philadelphia, Pa.
- Jennings, W. H., Head, W. J. & Mannings, C. R. (1976) A mechanistic model for the prediction of ductile erosion. Wear, 40, 93.
- Jones, M. H. & Lewis, R. (1979) Solid particle erosion of a selection of alloy steels. In: Proc. 5th Int. Conf. on Erosion by Solid and Liquid Impact, paper 52. Cambridge, England.
- Kosel, T. H., Scattergood, R. O. & Turner, A. P. L. (1979) An electron microscope study of erosive wear. In: Wear of Materials (Ed. by K. C. Ludema, W. A. Glaeser & S. K. Rhee), p. 192. Am. Soc. Mech. Engrs., New York.
- Kosel, T. H., Turner, A. P. L. & Scattergood, R. O. (1978) Effects of particle size and shape on erosive wear mechanisms. In: Corrosion - Erosion Behavior of Materials (Ed. by K. Natesan), p. 146. Metallurgical Society of AIME, St. Louis, Missouri.

ORIGINAL PAGES IN  
OF POOR QUALITY

- Levy, A. V. (1979) The role of plasticity in erosion. In: Proc. 5th Int. Conf on Erosion by Solid and Liquid Impact, paper 39. Cambridge, England.
- Malkin, S. (1981) Correlation between solid particle erosion of metals and their melting energies. Wear, 68, 391.
- Rabinowicz, E. (1979) The wear equation for erosion of metals by abrasive particles at moderate speeds. In: Proc. 5th Int. Conf. on Erosion by Solid and Liquid Impact, paper 38. Cambridge, England.
- Rickerby, D. G. & Macmillan, N. H. (1980) The erosion of aluminum by solid particle impingement at normal incidence. Wear, 60, 369.
- Ruff, A. W. (1980) Debris analysis of erosive and abrasive wear. In: Fundamentals of Tribology (Ed. by N. P. Suh & N. Saka), p. 877. MIT Press, Cambridge.
- Ruff, A. W. & Ives, L. K. (1975) Measurement of solid particle velocity in erosive wear. Wear, 35, 195.
- Salik, J. & Buckley, D. H. (1981a) Effect of erodant particle shape and various heat treatments on erosion resistance of plain carbon steel. NASA TP-1755, National Aeronautics and Space Administration, Washington, D.C.
- Salik, J. & Buckley, D. H. (1981b) Effect of mechanical surface and heat treatments on the erosion resistance. NASA TM-81540, National Aeronautics and Space Administration, Washington, D.C.
- Salik, J., Buckley, D. H. & Brainard, W. A. (1981) The effect of mechanical surface and heat treatments on the corrosion resistance of 6061 aluminum alloy. Wear, 65, 351.
- Schmitt, Jr., G. F. (1980) Liquid and solid particle impact erosion. In: Wear Control Handbook (Ed. by M. P. Peterson & W. O. Winer), p. 231. Am. Soc. Mech. Engrs., New York.
- Sheldon, G. L. (1977) Effects of surface hardness and other material properties on erosive wear of metals by solid particles. J. Eng. Mater. Technol. 99, 133.
- Smeltzer, C. E., Gulden, M. E. & Compton, W. A. (1970) Mechanisms of metal removal by impacting dust particles. J. Basic Eng. 92, 639.
- Soderberg, S., Hogmark, S. & Swahan, H. (1982) Mechanisms of material removal during erosion of a stainless steel. ASLE preprint no. 82-AM-4A-1.
- Tilly, G. P. (1969a) Erosion caused by airborne particles. Wear, 14, 63.
- Tilly, G. P. (1969b) Sand erosion of metals and plastics: a brief review. Wear, 14, 241.
- Tilly, G. P. (1973) A two-stage mechanism of ductile erosion. Wear, 23, 87.
- Tilly, G. P. (1979) Erosion by impact of solid particles. In: Treatise on Materials Science and Technology, vol. 13, (Ed. by U. Scott), p. 287. Academic Press, London.
- Tuitt, D. A. (1974) Erosion tests of metallic coatings. In: Proc. 4th Int. Conf. Rain Erosion (Ed. by A. A. Fyall & R. B. King), p. 677. Royal Aircraft Establishment, Farnborough, England.
- Veerabhadra Rao, P., Young, S. G. & Buckley, D. H. (1982a) Morphology of ductile metals eroded by a jet of spherical erodant particles impinging at normal incidence. NASA E-1092.
- Veerabhadra Rao, P., Young, S. G. & Buckley, D. H. (1982b) Morphology of an aluminum alloy eroded by a jet of angular particles impinging at normal incidence. NASA E-1166.
- Vijh, A. K. (1976) Resistance of metals to erosion by solid particles in relation to the solid state cohesion of metals. Wear, 39, 173.
- Wood, C. D. & Espenschade, P. W. (1965) Mechanisms of dust erosion. SAE Trans. 73, 515.

# ORIGINAL PAGE IS OF POOR QUALITY

TABLE I. - CHEMICAL COMPOSITION OF TEST MATERIALS

Material	Aluminum	Copper	Iron	Carbon	Manganese	Phosphorus	Sulfur	Magnesium	Silicon	Nickel
aluminum alloy 6061-T611 <sup>a</sup>	Balance	0.10-0.40	*****	*****	*****	*****	*****	0.05-1.2	0.4-0.8	0.10-0.20
Copper <sup>b</sup>	*****	99.9	*****	*****	*****	*****	*****	*****	*****	*****
Steel 1045 <sup>c</sup>	*****	*****	Balance	0.43-0.80	0.60-0.90	0.04 Max	0.05 Max	*****	*****	*****

- <sup>a</sup> Chao, C., Hammett, F. G., Kling, G. L. and Rogers, D. O. (1968) ASIM Round-Robin test with vibratory cavitation and liquid impact facilities of 6061-T611 aluminum alloy, 316 stainless steel, commercially pure nickel. Report No. MWP-68-1, The University of Michigan, Ann Arbor
- <sup>b</sup> Oxygen free, high conductivity (EPC) copper
- <sup>c</sup> Salik and Burkley (1981a)

TABLE II. - NOMINAL MECHANICAL PROPERTIES OF TEST MATERIALS

Material	Density, g/cm <sup>3</sup>	Tensile strength, M Pa	Yield strength, M Pa	Elongation, percent	Reduction in area, percent	Impact strength, joules	Hardness
Aluminum alloy 6061-T611 <sup>a</sup>	2.71	360	261	21.0	44	7.47	14 HRC
Copper	8.96	110-139	*****	*****	**	****	20 HRC
1045 Steel	7.85	600-720	401-429	49-61	**	****	51 HRC

- <sup>a</sup> Chao, et al. (1968)
- <sup>b</sup> Metals Handbook, T. Lyman, ed., Vol. 1, 8 ed., American Society for Metals, Metals Park, Novelty, Ohio

TABLE III. - CUMULATIVE VOLUME LOSS OF ALUMINUM ALLOY, COPPER AND 1045 STEEL SUBJECTED TO GLASS BEAD AND CRUSHED GLASS EROSION

Material	Cumulative volume loss in cm <sup>3</sup> after 10 minutes exposure	
	Glass beads	Crushed glass
Aluminum alloy	9.2	48.
Copper	10.0	41.
1045 steel	3.4	17.6

Standard deviation values for the experimental data scatter were observed to vary from 0.05 to 2.0%.

ORIGINAL PAGE IS  
OF POOR QUALITY

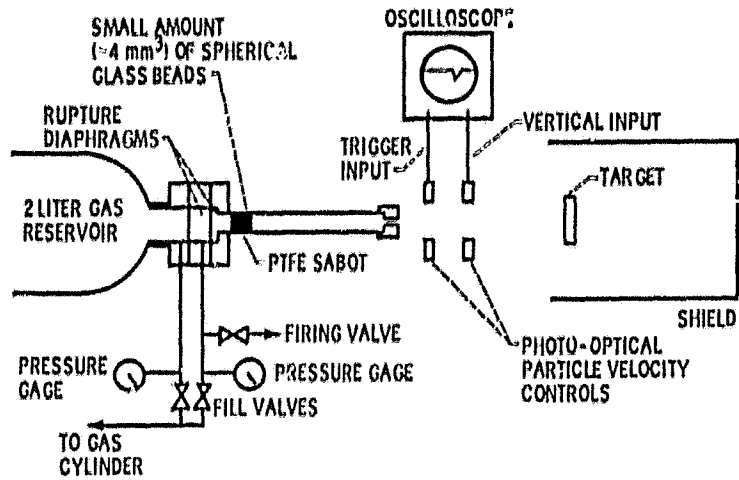


Figure 1. - Schematic of small-muzzle gun Impingement apparatus.

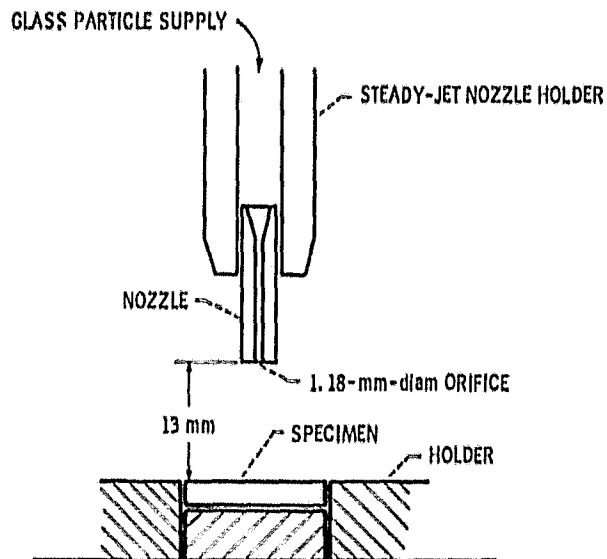
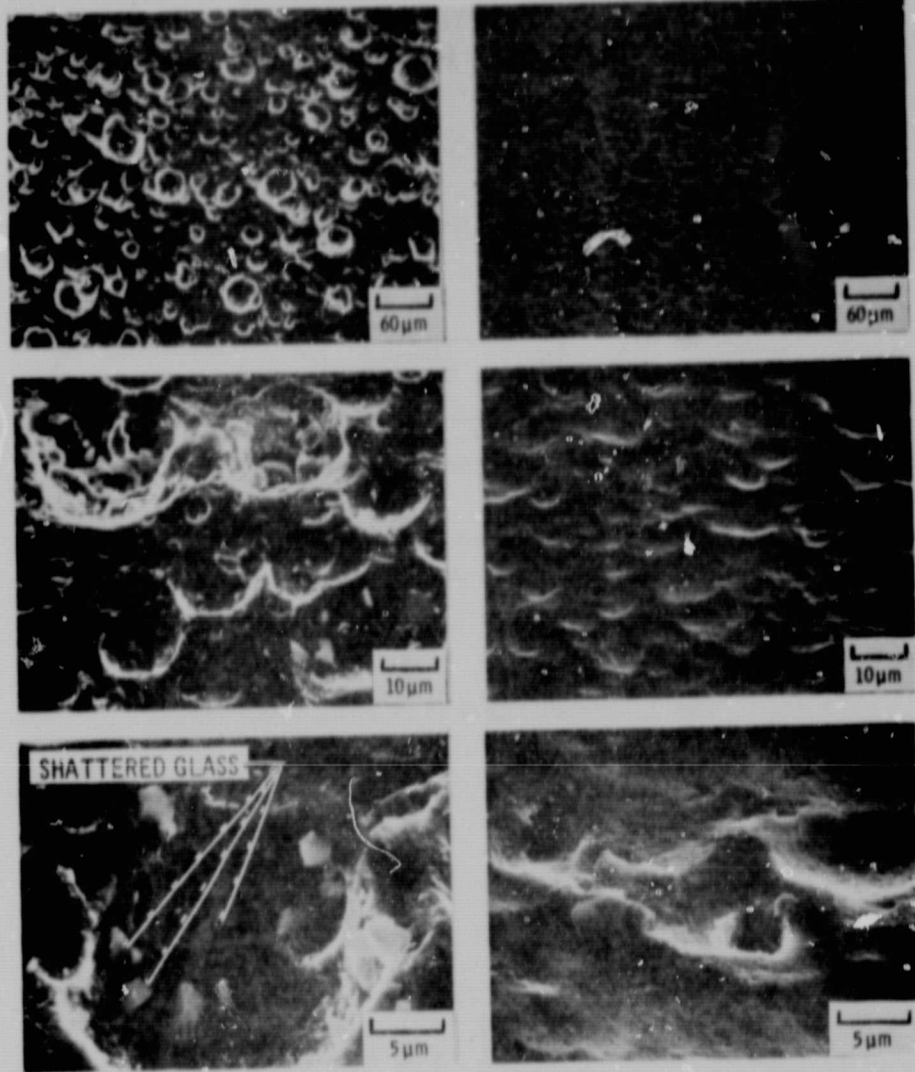


Figure 2. - Schematic diagram of steady-jet Impingement apparatus.

ORIGINAL PAGE  
BLACK AND WHITE PHOTOGRAPH



(a) Impulsive shattered glass.

(b) Steady jet impingement

Figure 3. - SEM micrographs of aluminum specimens exposed to two different types of impingement by glass.

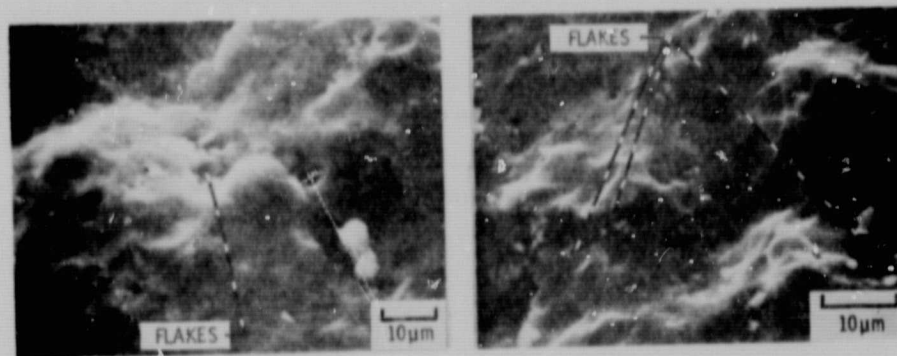


Figure 4. - SEM micrographs of aluminum specimen showing "Flakes".

ORIGINAL PAGE  
**BLACK AND WHITE PHOTOGRAPH**

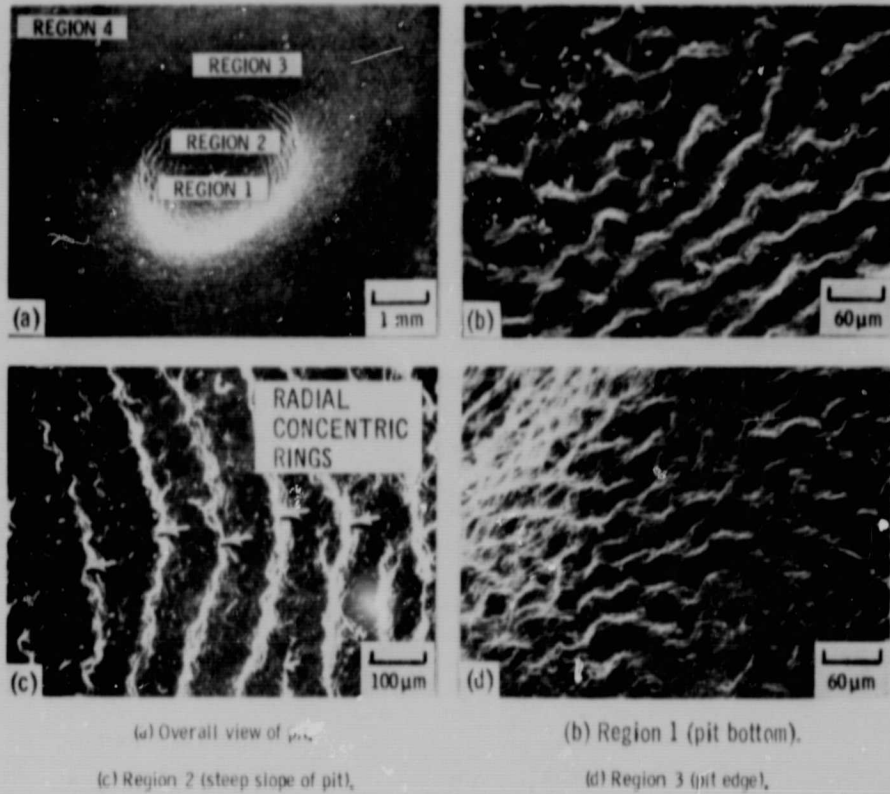


Figure 5. - SEM micrographs of aluminum specimen exposed to glass bead impingement for 10 minutes at 0.54 MPa pressure.

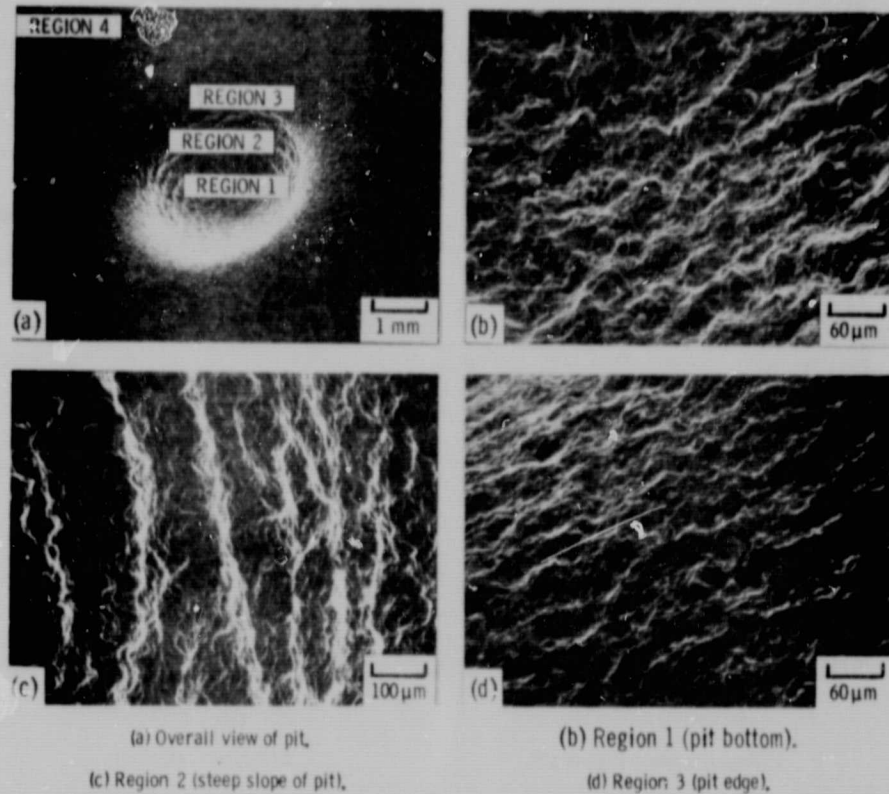
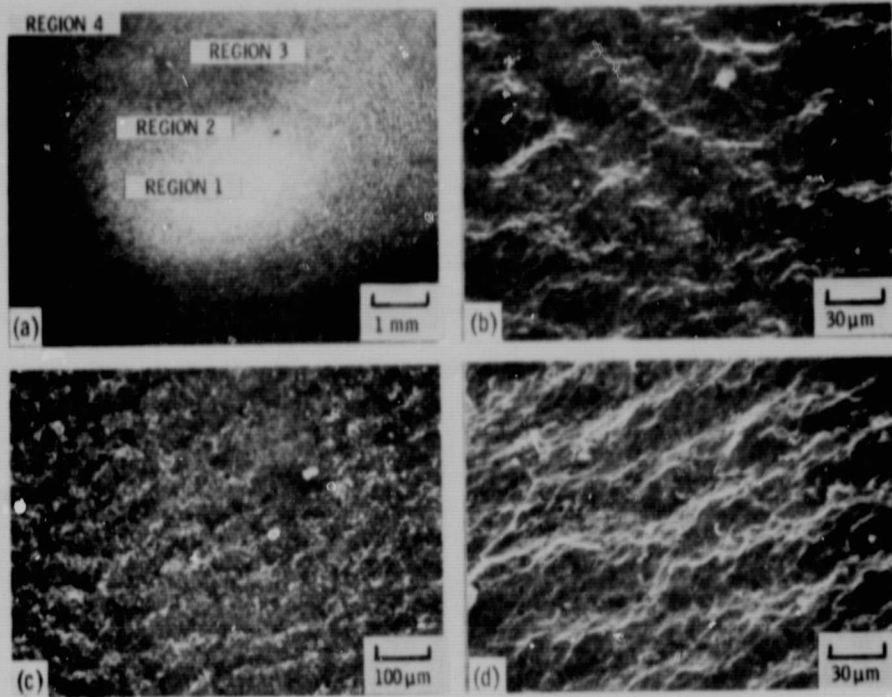


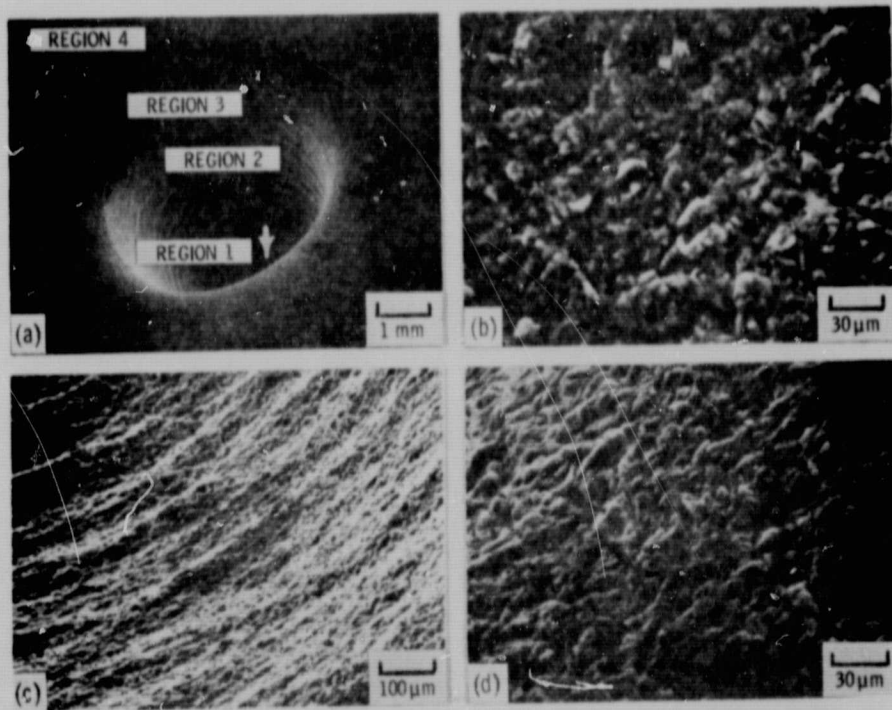
Figure 6. - SEM micrographs of copper specimen exposed to glass bead impingement for 10 minutes at 0.54 MPa pressure.

ORIGINAL PAGE  
BLACK AND WHITE PHOTOGRAPH



(a) Overall view of pit, (b) Region 1 (pit bottom),  
(c) Region 2 area (pit side), (d) Region 3 (pit edge).

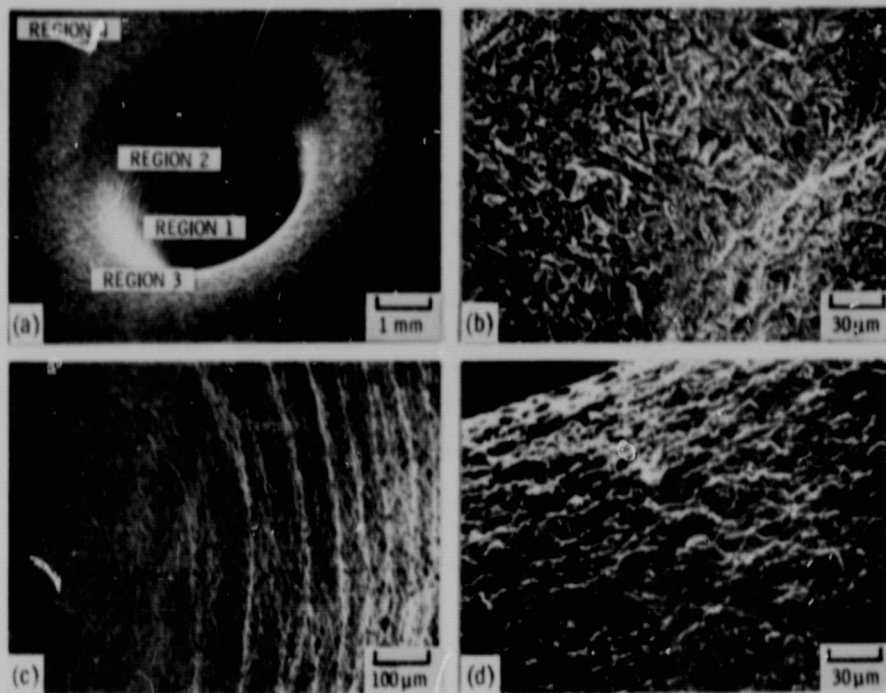
Figure 7. - SEM micrographs of 1045 steel specimen exposed to glass bead impingement for 10 minutes at 0.54 MPa pressure.



(a) Overall view of pit, (b) Region 1 (pit bottom),  
(c) Region 2 (steep slope of pit), (d) Region 3 (pit edge).

Figure 8. - SEM micrographs of aluminum specimen exposed to crushed glass impingement for 10 minutes at 0.54 MPa pressure.

ORIGINAL PAGE  
BLACK AND WHITE PHOTOGRAPH



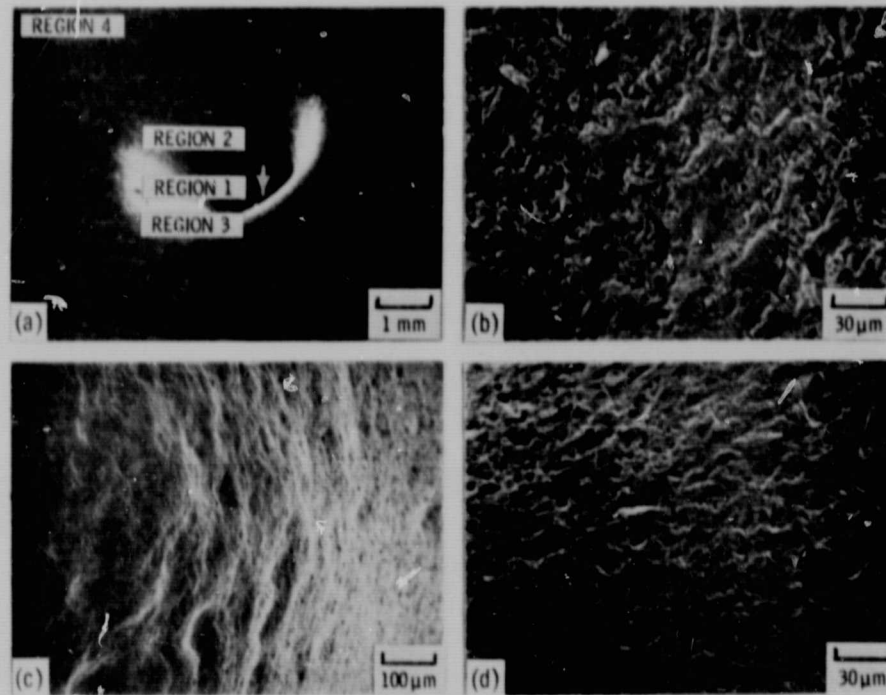
(a) Overall view of pit,

(c) Region 2 (steep slope of pit),

(b) Region 1 (pit bottom),

(d) Region 3 (pit edge),

Figure 9. - SEM micrographs of copper specimen exposed to crushed glass impingement for 10 minutes at 0.54 MPa pressure.



(a) Overall view of pit,

(c) Region 2 (steep slope of pit),

(b) Region 1 (pit bottom),

(d) Region 3 (pit edge),

Figure 10. - SEM micrographs of steel specimen exposed to crushed glass impingement for 10 minutes at 0.54 MPa pressure.

ORIGINAL PAGE  
BLACK AND WHITE PHOTOGRAPH

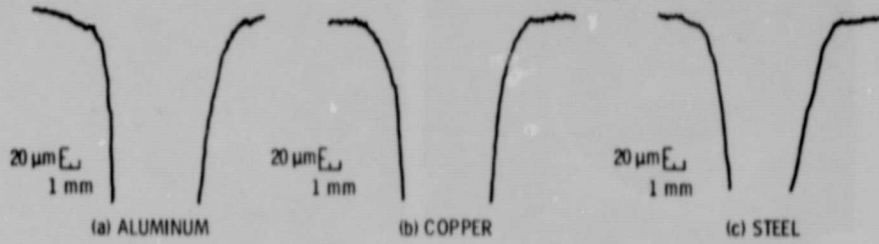


Figure 11. - Surface traces of aluminum, copper and steel specimens exposed to glass bead impingement for 10 min.

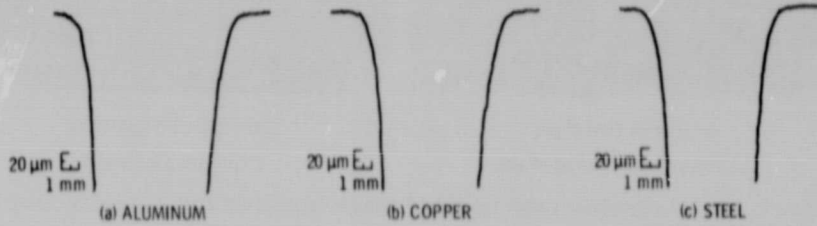
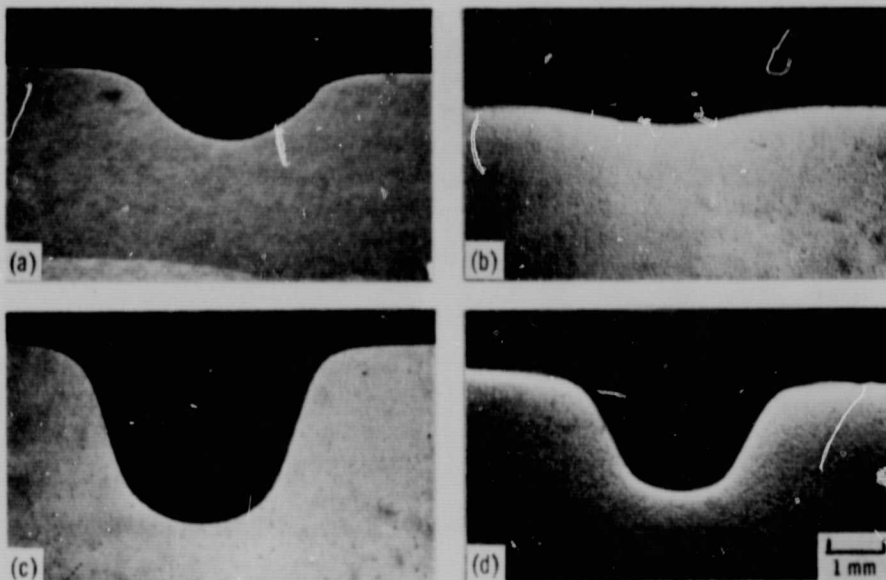


Figure 12. - Surface traces of aluminum, copper and steel specimens exposed to crushed glass impingement for 10 min.



(a) Aluminum - glass bead impingement. (b) 1045 steel - glass bead impingement.  
(c) Aluminum - crushed glass impingement. (d) 1045 steel - crushed glass impingement.

Figure 13. - Cross section of aluminum and 1045 steel specimens impacted with glass beads and crushed glass.

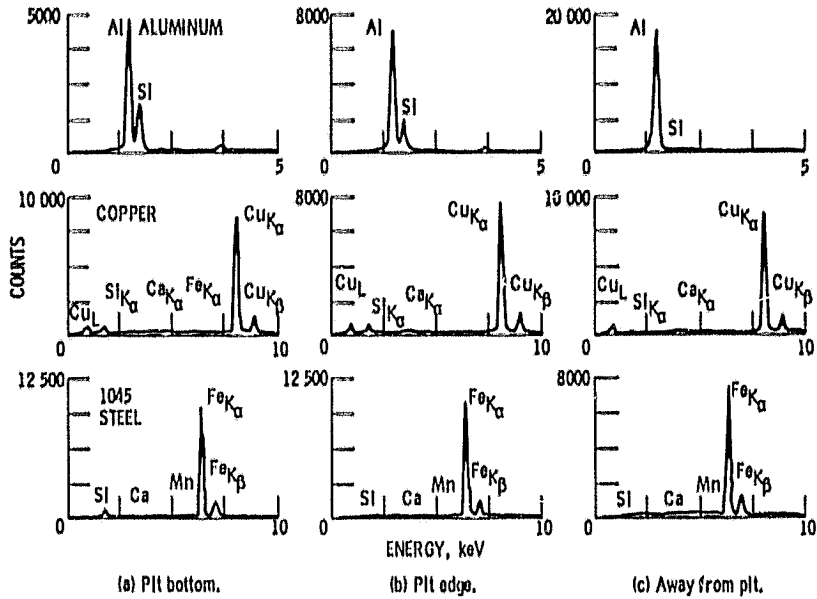


Figure 14. - EDS analysis of aluminum, copper and steel specimens exposed to glass bead impingement for 10 min at 0.54 MPa pressure.

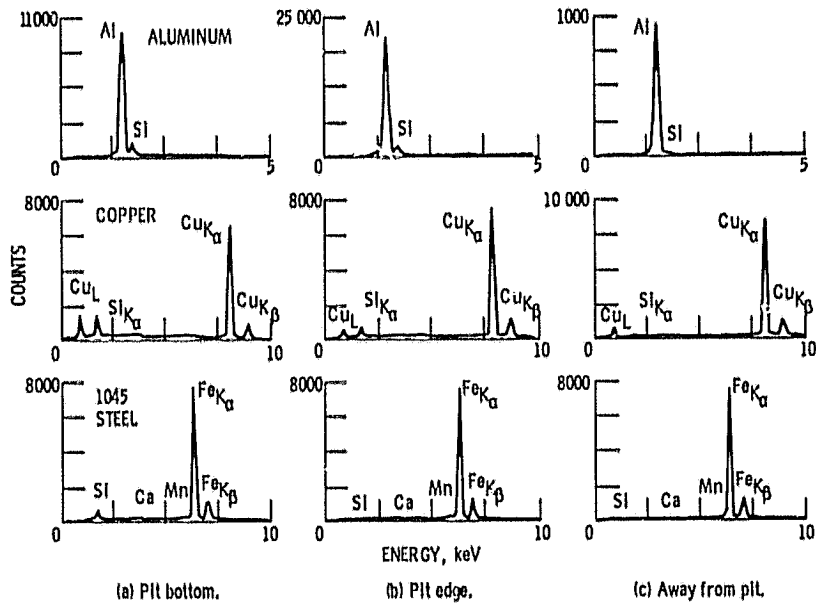


Figure 15. - EDS analysis of aluminum, copper and steel specimens exposed to crushed glass impingement for 10 min at 0.54 MPa pressure.